

# InAs/InP Quantum Dots in Etched Pits by Droplet Epitaxy in Metalorganic Vapor Phase Epitaxy


Elisa Maddalena Sala,\* Young In Na, Max Godsland, Aristotelis Trapalis, and Jon Heffernan

The growth of InAs quantum dots (QDs) on InP(100) via droplet epitaxy in a metalorganic vapor phase epitaxy (MOVPE) reactor is studied. Formation of indium droplets is investigated with varying substrate temperature, and spontaneous formation of nanoholes is observed for the first time under MOVPE conditions. Indium droplets are crystallized into QDs under arsenic flow at different temperatures. For temperatures greater than 500 °C, a local etching takes place in the QD vicinity, showing an unexpected morphology which is found to be strongly dependent on the crystallization conditions. Such QDs are structurally and optically investigated and emission from single QDs in the telecom C-band is detected via microphotoluminescence at low temperature.

In the last decades, self-assembled quantum dots (QDs) have attracted great attention due to their large impact on the performances of semiconductor lasers,<sup>[1,2]</sup> nanomemories,<sup>[3–6]</sup> and quantum information technologies.<sup>[7–9]</sup> In particular, III–V QDs are efficient sources of pure single photons<sup>[7]</sup> and entangled photon pairs,<sup>[10]</sup> and can be easily integrated into photonic chips, thus representing the building blocks for future quantum networks.<sup>[7,10]</sup> A successful and robust fabrication method for high-quality III–V QDs is the Stranski–Krastanov (SK) growth mode,<sup>[11]</sup> largely exploited in both molecular beam epitaxy (MBE) and metalorganic vapor phase epitaxy (MOVPE) environments.<sup>[12–14]</sup> An alternative technique is droplet epitaxy (DE), initially developed by Koguchi et al.<sup>[15]</sup> in MBE, which relies on the spontaneous formation of group III metallic droplets which are subsequently crystallized into QDs by the supply of a group V source. DE is a flexible technique for fabricating high-quality nanostructures, as it does not rely on the lattice-mismatch between substrate and epilayer, and its successful applications can be found for example in single-photon<sup>[16]</sup> and entangled pairs<sup>[17]</sup> emitters, and solar cells.<sup>[18]</sup>

Dr. E. M. Sala, Dr. A. Trapalis, Prof. J. Heffernan  
 EPSRC National Epitaxy Facility  
 Department of Electronic and Electrical Engineering  
 The University of Sheffield North Campus  
 Broad Lane, Sheffield S37HQ, UK  
 E-mail: e.m.sala@sheffield.ac.uk

Y. I. Na, M. Godsland  
 Department of Electronic and Electrical Engineering  
 The University of Sheffield North Campus  
 Broad Lane, Sheffield S37HQ, UK

 The ORCID identification number(s) for the author(s) of this article can be found under <https://doi.org/10.1002/pssr.202000173>.

DOI: 10.1002/pssr.202000173

One opportunity enabled by DE at high temperatures is the observation of metal-induced surface etching to create nucleation sites for further localization of QDs. This so-called local droplet etching (LDE) was first reported by Wang et al.<sup>[19]</sup> under MBE conditions. LDE is an appealing technique, as QDs positioned in the etched pits generally reveal narrow emission linewidths and small fine-structure-splitting (FSS)<sup>[20–22]</sup> due to increased spatial symmetry. This has fundamental advantages for achieving a higher degree of entanglement, by reducing the FSS of the excitons responsible for

entangled photon pair emission.<sup>[20]</sup> In contrast, much less attention has been devoted to DE in MOVPE,<sup>[23–29]</sup> where to date fabrication of QDs via SK still dominates. Nevertheless, recent development of DE in MOVPE produced high-quality InAs/InP QDs which have shown a smaller FSS compared with SK QDs<sup>[26]</sup> and led to demonstration of the first quantum light-emitting diode (QLED) operating around 1.55 μm at temperatures up to 93 K.<sup>[28]</sup> Among III–V QDs systems, InAs/InP QDs are indeed very attractive for fiber-based quantum network applications, due to their compatibility with the low-loss telecom C-band.

In this letter, we present a multi-step growth procedure for fabricating self-assembled InAs/InP QDs via DE in an MOVPE environment, leading to the formation of QDs in etched pits. The combination of DE and droplet etching is potentially advantageous as, unlike in previous MBE works, the infilling of etched pits in a separate step is not required. In fact, the droplet crystallization into QDs and the local etching take place at the same time. By adjusting the crystallization temperature, the etch depth around the QDs can be tuned and, at the same time, the QD morphology is considerably affected. We first consider the indium droplet formation on a bare InP surface and provide details on the growth sequence used for droplet crystallization into InAs QDs. Using a combination of atomic force microscopy (AFM), room temperature photoluminescence (RT-PL), and low temperature microphotoluminescence (LT-μPL), we investigate their morphological and optical properties.

The samples studied in this work were grown in a 3 × 2 close-coupled showerhead (CCS) Aixtron MOVPE reactor, using H<sub>2</sub> as carrier gas. The precursors used are trimethylindium (TMIn) for the indium droplets, phosphine (PH<sub>3</sub>), and arsine (AsH<sub>3</sub>), for InP growth and droplet crystallization into QDs, respectively. For droplet formation, indium was supplied at a constant TMIn flow of

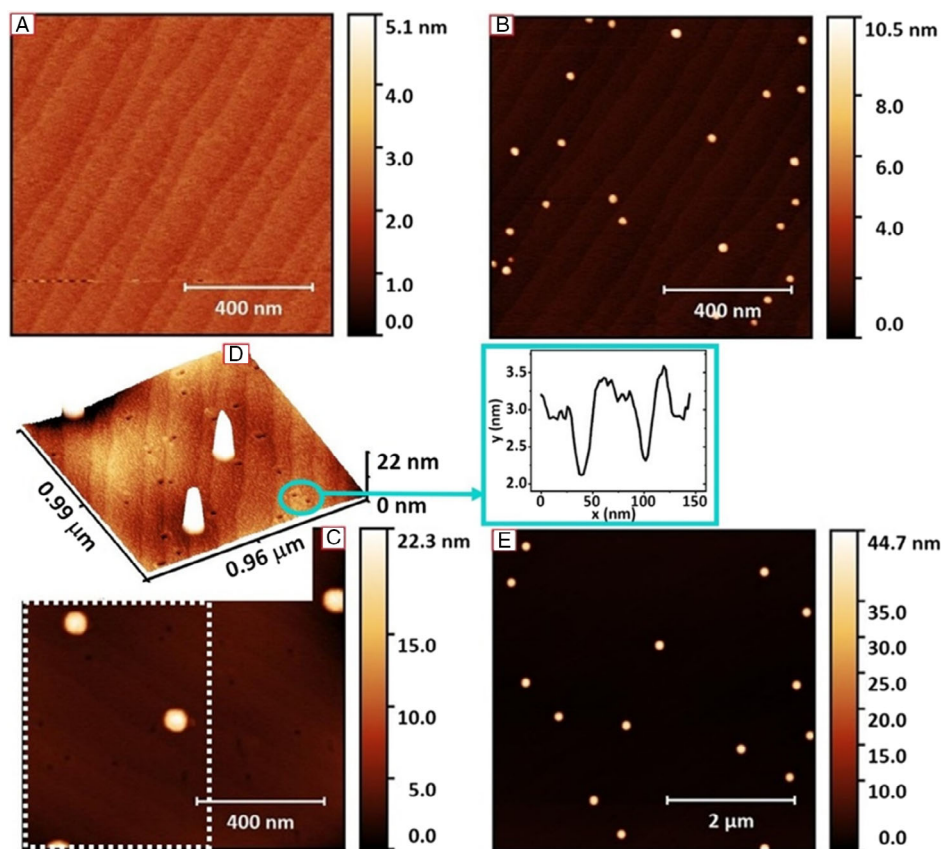


**Figure 1.** AFM images of indium droplets deposited on bare InP with increasing temperatures: A) 300 °C, B) 320 °C, C) 350 °C, E) 400 °C. In D) a 3D image of the dashed area in (C) is presented. Nanoholes are clearly visible: two of them are highlighted with a blue circle, and their profiles are also shown.

$2.6 \mu\text{mol min}^{-1}$  for 35 s after the growth of  $\approx 300$  nm InP buffer layer. **Figure 1** shows AFM images of indium droplets deposited on the bare InP (100) buffer surface, at substrate temperatures ranging from 300 to 400 °C. Indium droplets form and, as a result of metallic diffusion, the droplet density decreases with temperature from  $3 \times 10^9$  to  $6 \times 10^7 \text{ cm}^{-2}$  for 320 and 400 °C, respectively. Droplet dimensions vary accordingly, increasing proportionally with temperature from  $\approx(35 \pm 7)$  nm width and  $\approx(6 \pm 2)$  nm height to  $\approx(200 \pm 20)$  nm width and  $\approx(32 \pm 5)$  nm height for 320 and 400 °C, respectively. One limitation of DE in MOVPE is that the growth temperature and indium deposition are not independent, as they are in MBE,<sup>[30]</sup> and we observe that below 300 °C (Figure 1A), no droplets can be detected when the TMIn used as indium precursor material is not pyrolyzed. In Figure 1D, a 3D image shows a more detailed view of nanoholes that are formed on the InP surface, where indium droplets and nanoholes coexist. The typical nanohole depth is  $\approx(1 \pm 0.5)$  nm and  $\approx(30 \pm 5)$  nm wide, with density of  $\approx 10^9 \text{ cm}^{-2}$ . On closer inspection, the profiles of such holes strongly resemble the nanoholes spontaneously formed during DE in MBE, as reported for example in Wang et al.<sup>[19]</sup> To our knowledge, this is the first observation of such spontaneous nanoholes formation in MOVPE, when no group V flow is provided to the group III metallic droplets. Further experimental investigations are needed to confirm the exact physical mechanism behind the formation of such

nanoholes. Next, to study QD formation, indium droplets were exposed to an AsH<sub>3</sub> flow.

The full growth sequence is as follows: 1) growth of an InP buffer layer at 600 °C, 2) cooling down to droplet deposition temperature under PH<sub>3</sub> for surface stabilization, 3) indium deposition without any group V precursor for droplet formation, 4) heat up under an AsH<sub>3</sub> flow of  $24 \mu\text{mol min}^{-1}$ , 5) stabilization under AsH<sub>3</sub> for complete droplet crystallization, 6) InP capping layer at the same temperature, and 7) final InP layer to bury the QDs for PL emission. For AFM investigations, the growth procedure is terminated after the stabilization step (5), and the samples are immediately cooled down to room temperature. **Figure 2** shows AFM images of free-standing InAs QDs on bare InP surfaces, originating from crystallisation of droplets deposited at 320 °C (as in Figure 1B).

Here, the droplet crystallization temperature has been varied in the range 480–530 °C, and three main features can be distinguished with increasing temperature: 1) increase in QD density, 2) increase in the magnitude of the locally etched region around each QD, 3) alteration of QD size. In the temperature range used, the QD density varied from  $4 \times 10^8$  to a maximum of  $9 \times 10^8 \text{ cm}^{-2}$  at 520 °C, without supplying any additional material in terms of TMIn or AsH<sub>3</sub> flows. QD dimensions increase with temperature up to 520 °C, whereas a clear size reduction is observed at 530 °C, see Figure 2D.

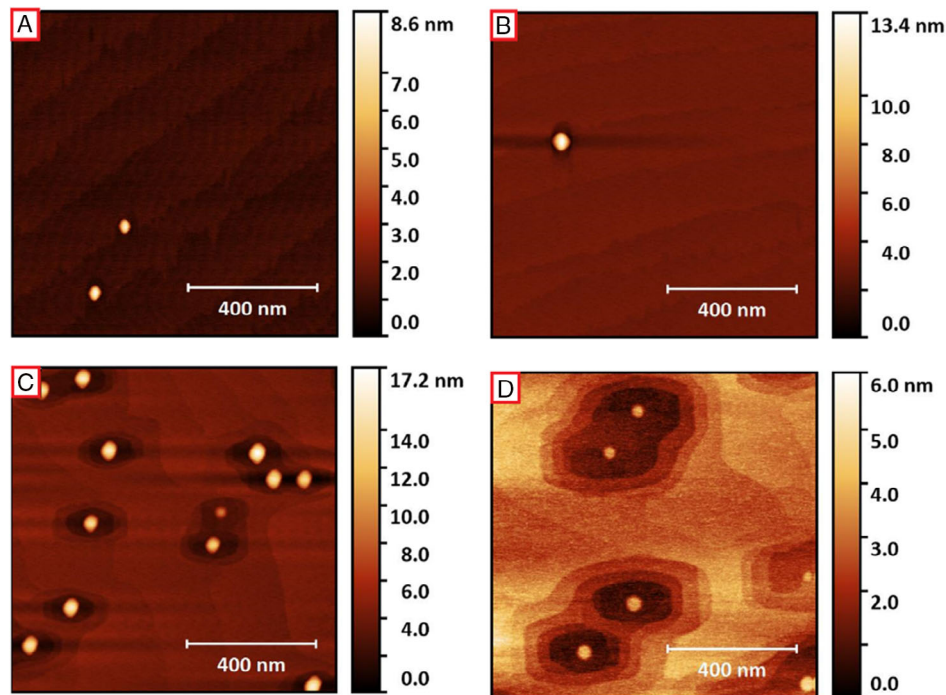


**Figure 2.** AFM images of free-standing InAs/InP QDs crystallized at different temperature: A) 480 °C, B) 500 °C, C) 520 °C, and D) 530 °C.

From analysis of a large number of dots, typical QD dimensions at 480 °C are  $\approx(5 \pm 2)$  nm and  $\approx(45 \pm 7)$  nm, for height and width, respectively. At 520 and 530 °C, QDs show a bimodal size distribution. At 520 °C, they have diameters of  $\approx(56 \pm 7)$  nm and  $\approx(45 \pm 5)$  nm and heights of  $\approx(15 \pm 3)$  nm and  $\approx(7 \pm 2)$  nm, respectively; whereas at 530 °C, diameters of  $\approx(60 \pm 5)$  nm and  $\approx(35 \pm 5)$  nm and heights of  $\approx(5 \pm 1.5)$  nm and  $\approx(2 \pm 0.5)$  nm, respectively are found. This means that from 520 to 530 °C the QD aspect ratio has strongly reduced ( $\approx -65\%$ ) for both QD populations. More detailed analysis is given in **Figure 3** which shows 3D AFM images of single (double) QDs and illustrates the formation of QDs within locally etched pits. These pits start to form at crystallization temperatures above 500 °C as also shown in **Figure 2B–D**. The pit depth increases from 1 nm at 500 °C to 1.8, 2.7, and 3.4 nm at 510, 520, and 530 °C, respectively. Interestingly, such profiles appear step-like, suggesting that the etching proceeds layer-wise, and the depth is a function of the crystallization temperature. The same holds true for the width and length which both increase with increasing temperature. In all cases, the etching areas are elongated, most likely due to the intrinsic stress asymmetry along the two crystallographic directions [0-1-1] and [0-11] at the InAs/InP interface<sup>[30]</sup> (note that the indium droplets themselves are not elongated, see **Figure 1**).

During the heating up and arsenic supply steps (4) and (5), no phosphorus for surface stabilization is provided, and the InP surface is In-rich due to the metallic indium previously deposited. Hence, it is very likely that at temperatures as high as 500 °C, it becomes unstable and thus InP can easily dissolve into indium and phosphorus atoms, particularly underneath and close to the indium droplets, similarly to what is observed for DE in MBE conditions.<sup>[19]</sup> The more the temperature rises, i.e., from 500

to 520 °C, the more InP dissolves and the more indium atoms contribute to increasing the droplets' size, resulting in bigger QDs. The dissolved P atoms instead would likely escape into the growth chamber. Note that the In–P bond strength is smaller than In–As, i.e.,  $\approx 47.3$  versus  $\approx 48.0$  kcal mol<sup>-1</sup><sup>[31,32]</sup> thus favoring the formation of InAs as part of the QDs over InP, once the In–P bonds are broken. Further increasing the temperature from 520 to 530 °C leads to a higher probability for indium atoms to have enough energy to escape from the droplets, thus not contributing to the formation of the final QDs; hence, the crystallized QDs will appear smaller. It has been previously observed that for InAs QDs grown on InP via DE in MOVPE, a nonstoichiometric 2D layer is formed during the indium droplet exposure to the arsenic flow during the temperature ramp,<sup>[26]</sup> here denoted as step (4) of the growth sequence. Such a layer is expected to be formed due to As–P exchange reactions while exposing the In-rich InP surface to arsenic.<sup>[33]</sup> It is referred to as a “2D quasi-wetting layer” (WL) and is likely made of InAs<sub>x</sub>P<sub>1-x</sub>.<sup>[26]</sup> This differs from the common WL found in SK QDs, where strain accumulates and is subsequently released via formation of 3D islands.<sup>[11,12]</sup> From **Figure 3**, it is plausible that the step-like etching is due to parts of such InAs<sub>x</sub>P<sub>1-x</sub> layer in proximity to the QDs being etched away. Evidence for this is seen in **Figure 4** where we present room temperature macro PL spectra from the samples. Samples were excited with a 645 nm diode laser at 75 Wcm<sup>-2</sup> power density. Various emission lines can be detected, which are labeled A, B, C, and D. Peak A is found in all samples at the same spectral position and is attributed to the InP substrate ( $\approx 920$  nm at RT<sup>[34]</sup>), and the broad emission band D is attributed to QD emission. It is important to point out that, due to the specific physical properties

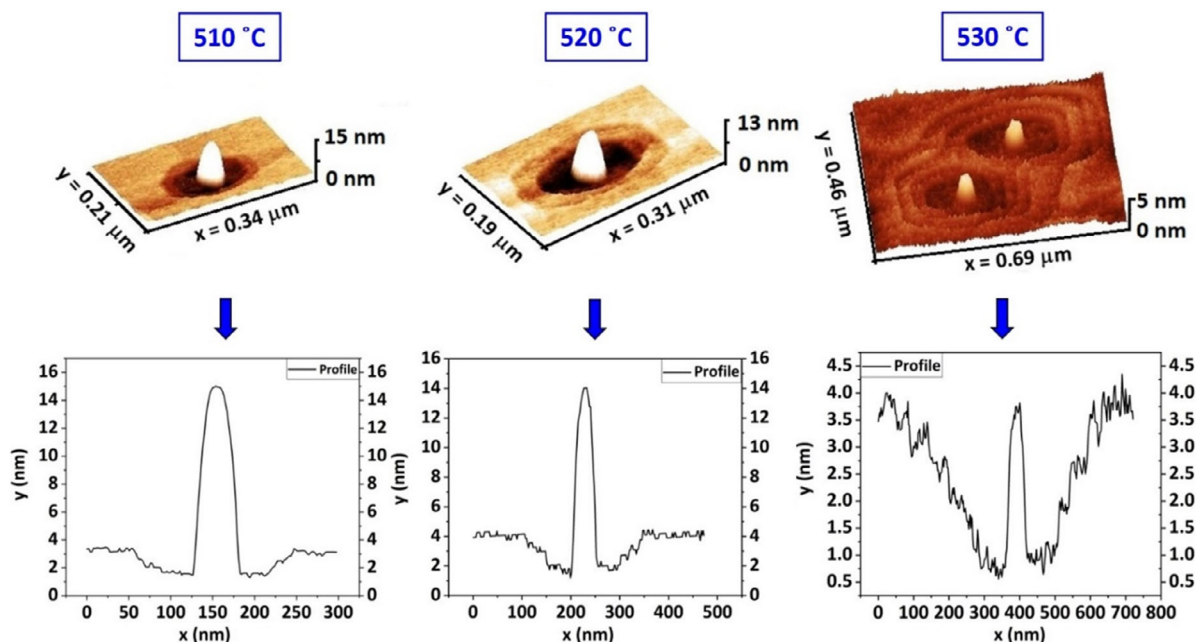


**Figure 3.** 3D AFM images of QDs and related profiles as a function of crystallization temperature. The lateral dimensions of the etch pits for the considered temperatures are the following:  $T = 510\text{ °C}$ :  $(150 \pm 10)\text{ nm}$  and  $(100 \pm 10)\text{ nm}$ .  $T = 520\text{ °C}$ :  $(240 \pm 20)\text{ nm}$  and  $(130 \pm 20)\text{ nm}$ .  $T = 530\text{ °C}$ :  $(450 \pm 50)\text{ nm}$  and  $(230 \pm 20)\text{ nm}$ .

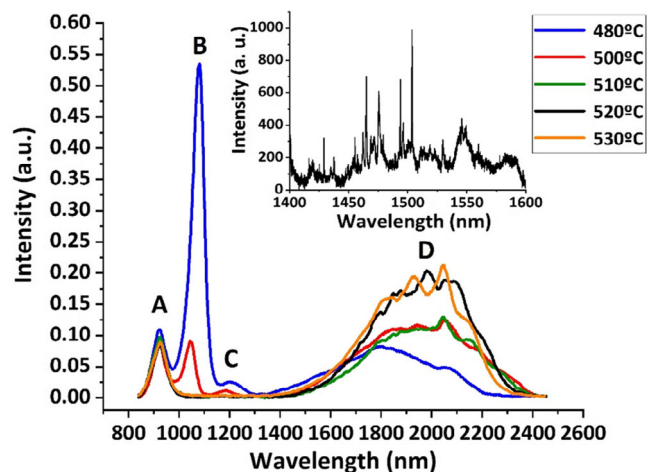


**Figure 4.** RT-PL of QD samples crystallized at temperatures ranging from 480 to 530 °C. The inset displays  $\mu$ PL measurements carried out at 4 K, relatively to the sample grown at 520 °C.

of the InAs/InP system (lower lattice mismatch compared with the widely studied InAs/GaAs, i.e.,  $\approx 3\%$  vs  $\approx 7\%$ ), the resulting QDs are bigger in size compared with InAs QDs on GaAs. Hence, we expect QDs grown at these conditions to emit at longer wavelength than  $1.5\ \mu\text{m}$  at room temperature, as already observed in previous studies.<sup>[35]</sup> Moreover, the additional contribution in the range 1900–2300 nm seen at  $T \geq 500\text{ °C}$  confirms the QD size increase observed in our AFM investigations. Peaks B and C, we attribute to emission from the 2D quasi-WL emission. Interestingly, both these peaks blueshift with increasing

droplet crystallization temperature and are eventually completely quenched at 520 °C. In particular, peak B emits at 1074 nm for the sample grown at 480 °C, then blueshifts to 1041 nm and finally to 1008 nm for 500 and 510 °C, respectively. At greater temperatures, its emission cannot be distinguished anymore from the background. Peak C shifts in a similar manner, whereas at the same time, the QD emission D gains intensity ( $\approx 50\%$  more for 520 °C compared to 480 °C), suggesting a more efficient carrier recombination into the QDs. We hypothesize that the blueshift and the quenching of peaks B and C correspond to the increased magnitude of the etching around the QDs as observed in the AFM investigations. From the AFM analysis, we can estimate the total etched area per  $1\ \mu\text{m}^2$ : it amounts to  $\approx 0.1$ ,  $\approx 0.3$ , and  $0.6\ \mu\text{m}^2$  for 510, 520, and 530 °C, respectively. Hence, with increasing temperature, the stepped etching process seen in Figure 3 leads to a gradual reduction in the average thickness of the 2D layer (the blue shift), and the overall contribution of this layer to the PL decreases as the etch pit size increases and the total area of the 2D layer decreases. Finally, it is important to note that such emission is still detectable at low temperatures (not shown here), which indicates that a contribution to the emission from the 2D layer is still present, but overall much weaker due to the etching.

Finally, in the inset of Figure 4, we present LT- $\mu$ PL from the QDs crystallized at 520 °C. The measurement has been carried out using a 635 nm laser, and a power density of  $4.5\ \text{W cm}^{-2}$  at 4 K. Emission from single QDs can be clearly detected which confirms the attribution of peak D to QD emission. It is worth pointing out that single dot emission is not observed for QDs crystallized at temperatures below 520 °C nor at 530 °C. Micro-PL for these samples instead shows a broad emission but no sharp lines

characteristic of single dot emission. In both cases, we believe this is due to the presence of significant charge noise which leads to a severe broadening and coalescence of emission peaks.<sup>[36]</sup> In the case of the lower temperature samples, this is likely due to the effect of the quasi-2D WL which, as can be seen from macro-PL, is still an efficient layer for carrier capture. For the 530 °C sample, it may be due the presence of point defects associated with the AsH<sub>3</sub>-stabilized InP surface, as reported by Masut et al.<sup>[37]</sup> Therefore, we believe that 520 °C constitutes the optimum temperature for droplet crystallization into high-quality InAs QDs, which can be therefore clearly measured by  $\mu$ PL. Spectra from the sample show a broad range of linewidths up to 125  $\mu$ eV, but a significant proportion of QDs have linewidths less than the 45  $\mu$ eV resolution of the spectrometer. The observation of narrow linewidth single QD emission indicates the high quality of these DE crystallized QDs in MOVPE, and with further growth optimization, we expect the QDs to be suitable for quantum optics applications, especially in controlling the exciton FSS, crucial for photon entanglement.<sup>[20]</sup>

In conclusion, we studied the formation of InAs QDs on bare InP (100) surfaces by DE in MOVPE. By varying the droplet crystallization temperature, the QD structural properties are considerably altered. In particular, QDs grown at temperatures greater than 500 °C are positioned in locally etched pits, whose size is directly proportional to the crystallization temperature. Structural and optical investigations show a clear correlation between the etching magnitude and the emission intensities of the 2D-layer and the QD band at room temperature, suggesting that the local etching leads to a more efficient carrier capture into QDs, especially for crystallization temperatures of 520 and 530 °C. In addition, micro-PL investigations showed emission of single QDs around 1.55  $\mu$ m, with a proportion of dots exhibiting linewidths less than the 45  $\mu$ eV resolution of our spectrometer, thus confirming good optical quality in the telecom C-band and opening the path for their use in quantum optics applications. We believe that controlling a growth process that combines DE and droplet etching could lead to improvement in the QD optical properties, and in particular to a reduction in the QD FSS, a key parameter governing the degree of entanglement in single photon pairs.<sup>[20]</sup> This study represents therefore an important step in the MOVPE growth of high-quality InAs QDs in etched pits emitting at telecom wavelengths. Moreover, the etching process studied here may also be used as a “defect removal” procedure for DE QDs positioned in prepatterned hole templates, as most patterning techniques inadvertently introduce defects and impurities.<sup>[38]</sup>

## Acknowledgements

The authors wish to thank Dr Joanna Skiba-Szymanska (Toshiba Research Europe Limited, Cambridge, UK) for fruitful discussions and advice. This work was supported by EPSRC, Grant No. EP/R03480X/1 and by the InnovateUK project Aquasec. The data supporting the findings of this study are openly available in the University of Sheffield data repository at <https://doi.org/10.15131/shef.data.12063936>.

## Conflict of Interest

The authors declare no conflict of interest.

## Keywords

atomic force microscopy, droplet epitaxy, III–V quantum dots, metalorganic vapor phase epitaxy, photoluminescence

Received: April 6, 2020

Revised: May 1, 2020

Published online:

- [1] N. N. Ledentsov, *Semicond. Sci. Technol.* **2011**, *26*, 014001.
- [2] D. Bimberg, U. W. Pohl, *Mater. Today* **2011**, *14*, 388.
- [3] D. Bimberg, M. Geller, A. Marent, T. Nowozin, *US Patent 8331142 B2*, **2012**.
- [4] A. Marent, T. Nowozin, J. Gelze, F. Luckert, D. Bimberg, *Appl. Phys. Lett.* **2009**, *95*, 242114.
- [5] L. Bonato, E. M. Sala, G. Stracke, T. Nowozin, A. Strittmatter, M. N. Ajour, K. Daqrouq, D. Bimberg, *Appl. Phys. Lett.* **2015**, *106*, 042102.
- [6] E. M. Sala, I. F. Arikan, L. Bonato, F. Bertram, P. Veit, J. Christen, A. Strittmatter, D. Bimberg, *Phys. Status Solidi B* **2018**, *255*, 1800182.
- [7] P. Michler, *Quantum Dots for Quantum Information Technologies*, Springer, Berlin/New York **2017**.
- [8] D. Castelvetti, *Nature* **2017**, *541*, 9.
- [9] A. J. Shields, *Nat. Photonics* **2007**, *1*, 215.
- [10] N. Akopian, N. H. Lindner, E. Poem, Y. Berlatzky, J. Avron, D. Gershoni, B. D. Gerardot, P. M. Petroff, *Phys. Rev. Lett.* **2006**, *96*, 130501.
- [11] V. A. Shchukin, N. N. Ledentsov, D. Bimberg, *Epitaxy of Nanostructures*, Springer, Berlin/New York **2003**.
- [12] D. Bimberg, M. Grundmann, N. N. Ledentsov, *Quantum Dot Heterostructures*, Wiley, Chichester **1999**.
- [13] P. M. Petroff, S. P. Den Baars, *Superlattices Microstruct.* **1994**, *15*, 1.
- [14] T. Fukui, S. Ando, Y. Tokura, T. Toriyama, *Appl. Phys. Lett.* **1991**, *58*, 2018.
- [15] N. Koguchi, S. Takahashi, T. Chikyow, *J. Cryst. Growth* **1991**, *111*, 688.
- [16] E. Stock, T. Warming, I. Ostapenko, S. Rodt, A. Schliwa, J. Amaru Töfflinger, A. Lochmann, A. I. Toropov, S. A. Moshchenko, D. V. Dmitriev, V. A. Haisler, D. Bimberg, *Appl. Phys. Lett.* **2010**, *96*, 093112.
- [17] N. Ha, T. Mano, T. Kuroda, Y. Sakuma, K. Sakoda, *Appl. Phys. Lett.* **2019**, *115*, 083106.
- [18] P. Yu, J. Wu, L. Gao, H. Liu, Z. Wang, *Sol. Energy Mater. Sol. Cells* **2017**, *161*, 377.
- [19] Z. M. Wang, B. L. Liang, K. A. Sablon, G. J. Salamo, *Appl. Phys. Lett.* **2007**, *90*, 113120.
- [20] M. Gurioli, Z. Wang, A. Rastelli, T. Kuroda, S. Sanguinetti, *Nat. Mater.* **2019**, *18*, 799.
- [21] Y. H. Huo, A. Rastelli, O. G. Schmidt, *Appl. Phys. Lett.* **2013**, *102*, 152105.
- [22] C. Heyn, A. Stemmann, T. Köppen, Ch Strelow, T. Kipp, M. Grave, S. Mendach, W. Hansen, *Appl. Phys. Lett.* **2009**, *94*, 183113.
- [23] Y. Nonogaki, T. Iguchi, S. Fuchi, Y. Fujiwara, Y. Takeda, *Mater. Sci. Eng.* **1998**, *B51*, 118.
- [24] J. Sormunen, J. Riikonen, M. Mattila, J. Tiilikainen, M. Sopanen, H. Lipsanen, *Nano Lett.* **2005**, *5*, 1541.
- [25] T. Ujihara, Y. Yoshida, W. S. Lee, Y. Takeda, *Appl. Phys. Lett.* **2006**, *89*, 083110.
- [26] J. Skiba-Szymanska, R. M. Stevenson, C. Varnava, M. Felle, J. Huwer, T. Müller, A. J. Bennett, J. P. Lee, I. Farrer, A. B. Krysa, P. Spencer, L. E. Goff, D. A. Ritchie, J. Heffernan, A. J. Shields, *Phys. Rev. Appl.* **2017**, *8*, 014013.

- [27] A. Shikin, E. Lebedkina, C. Ciostek, P. Holewa, S. Ndoni, K. Almdal, K. Yvind, M. Syperek, E. Semenova, *Opt. Mater. Express* **2019**, 9, 1738.
- [28] T. Müller, J. Skiba-Szymanska, A. B. Krysa, J. Huwer, M. Felle, M. Anderson, R. M. Stevenson, J. Heffernan, D. A. Ritchie, A. J. Shields, *Nat. Commun.* **2018**, 9, 862.
- [29] H. Liu, Y. Jin, C. Yang, *CrystEngComm* **2016**, 18, 4499.
- [30] D. Fuster, K. Abderrafi, B. Alén, Y. González, L. Wewior, L. González, *J. Cryst. Growth* **2016**, 434, 81.
- [31] S. Anantathanasarn, R. Nötzel, P. J. van Veldhoven, T. J. Eijkemans, J. H. Wolter, *J. Appl. Phys.* **2005**, 98, 013503.
- [32] Y. R. Luo, *Comprehensive Handbook of Chemical Bond Energies*, CRC Press, Boca Raton FL **2007**.
- [33] N. Kobayashi, Y. Kobayashi, *J. Cryst. Growth* **1992**, 124, 525.
- [34] M. Bugajski, W. Lewandowski, *J. Appl. Phys.* **1985**, 57, 521.
- [35] S. Hasan, H. Han, M. Korytov, M. Pantouvaki, J. Vanampenhout, C. Merckling, W. Vandervorst, *J. Cryst. Growth* **2020**, 531, 125342.
- [36] J. Houel, A. V. Kuhlmann, L. Greuter, F. Xue, M. Poggio, B. D. Gerardot, P. A. Dalgarno, A. Badolato, P. M. Petroff, A. Ludwig, D. Reuter, A. D. Wieck, R. J. Warburton, *Phys. Rev. Lett.* **2012**, 108, 107401.
- [37] R. A. Masut, M. A. Sacilotti, A. P. Roth, D. F. William, *Can. J. Phys.* **1987**, 65, 1047.
- [38] H. Lan, Y. Ding, *Nano Today* **2012**, 7, 94.